Suspended sediment load and bedload flux from the Glacier d'Otemma proglacial forefield (summers 2020 and 2021)

D. Mancini[1], M. Dietze[2,3], M. Jenkin[1], F. Miesen[1] and S.N. Lane[1]

[1] Institute of Earth Surface Dynamics (IDYST), Université de Lausanne, Lausanne, Switzerland.
[2] Institute of Geography, Georg-August-University Göttingen, Göttingen, Germany.
[3] German Research Center for Geosciences (GFZ), Potsdam, Germany.

1. Introduction

The Glacier d'Otemma proglacial margin, located in the Swiss Alps at an altitude of about 2450 m a.s.l. (45.93423 N, 7.41160 E), is characterized by a ca. 1 km long by 200 m wide active braided forefield (Figure 1). In this setting we installed two gauging stations for the monitoring of both suspended sediment and bedload transport within the proglacial margin: GS1 at about 350 m from the glacier terminus and GS2 at the forefield outlet.

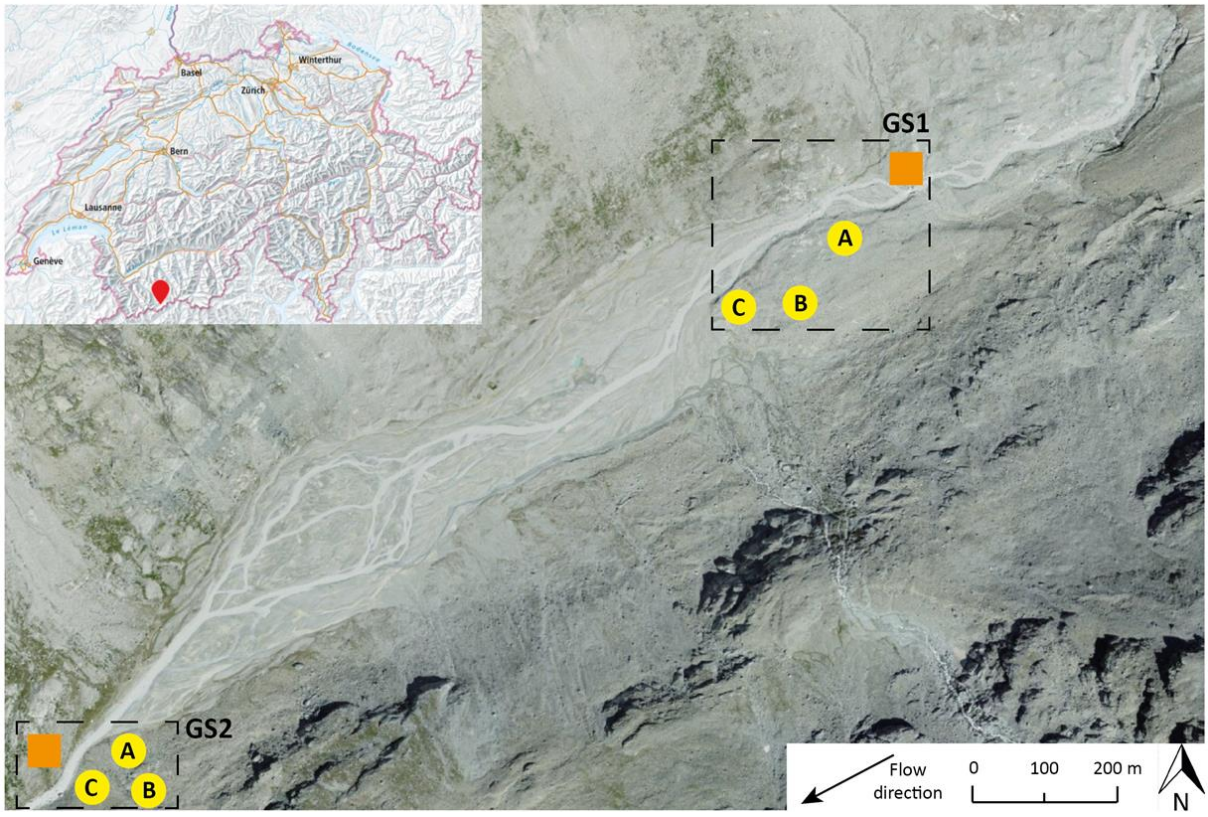

Figure 1: Glacier d'Otemma proglacial forefield with location of gauging station (GS) 1 and 2. Yellow dots refers to the location of geophones, while orange squares to turbidity and water stage probes. Source of background images: Swisstopo.

Monitoring stations were equipped with water pressure sensors (CS451 from Cambell Scientific), turbidity probes (OBS300+ from Cambell Scientific) and geophones (3-components PE-6/B from Sensor Nederland connected to a DiGOS DATA-CUBE type 2 logger). Water discharge were determined following modalities described in Müller and Miesen (2022). Suspended loads were quantified using a conventional turbidity-suspended sediment concentration relationship, while bedload transport was derived seismically using the geophysical Fluvial model inversion (FMI) algorithm developed in Dietze et al. (2018). The dataset covers two melt seasons characterized by different climatic conditions: summer 2020 from June 25th (Julian Day [JD] 177) to August 29th (JD 242), which was warmer and drier; and

summer 2021 from June 11th (JD 162) to August 21st (JD 233), which was colder and wetter especially in the first part of the season. Here a brief description of the methodology used to obtain sediment transport quantifications is given, but further details are available in Mancini et al. (2023).

2. Suspended sediment load transport

Turbidity records were automatically collected at a sampling frequency of 2 minutes. In 2020 we installed single probes at both stations, while in 2021 we had two probes per location (one installed above the other) to deal with burial problem. For each year, and for each gauging station, we developed a specific calibration curve describing the relation between manually collected suspended sediment concentration through the USDH-48 technique [g/l] and recorded turbidity [NTU]. These were fitted using robust regression using the iteratively-reweighted least squares (IRLS) method after Beaton and Tukey (1974) (also known as the bi-square method). For both stations in 2020 and 2021 we observed the relationship between turbidity and concentration to be linear as expected for the range of concentrations sampled given the probe specification, thus we fitted first order polynomials (y = ax+b, where y is the concentration [g/l] and x is the turbidity [NTU]). The obtained R^2 values between the two variables are generally very high. The results are shown in Table S1.

Table 1: Summary of suspended sediment calibration and analysis results. GS2 data in 2021 are divided into two periods because of burial problems and sensor failure: the higher probe was used until the 6th August and the lower probe from the 6th August.

Date	**2020**		**2021**	
Site	**GS1**	**GS2**	**GS1**	**GS2 Period 1; Period 2**
Start date	25th June	26th June	10th June	10th June
End date	14th September	14th September	8th September	8th September
Analysis period after cleaning	26th June 31st August	26th June 31st August	10th June 21st August	10th June 21st August
Percentage of record common to both stations after cleaning	89.6%		90.0%	
Manual suspended sediment samples	66	67	45	28; 30
a	0.0040	0.0032	0.0038	0.0072; 0.0043
b	0.467	-0.007	0.180	-0.107; 0.026
R^2	85.3 %	91.7 %	93.5%	85.8%; 77.1%

The calibration curves were then combined with the cleaned turbidity data to estimate time-series of concentration (C_i, where i is the time stamp). For each fit, confidence intervals were used to determine the uncertainty in concentration for each estimation ($\sigma_{C,i}$). The instantaneous load was calculated for each time period as Q_iC_i, where Q_i is the instantaneous discharge rate measured in Müller and Miesen (2022). We applied a product rule (Taylor, 1997) to estimate the associated uncertainty ($\sigma_{QC,i}$) under the assumption that the errors are Gaussian and independent:

$$\sigma_{QC,i} = \pm Q_i C_i \left[\left(\frac{\sigma_{Q,i}}{Q_i} \right)^2 + \left(\frac{\sigma_{C,i}}{C_i} \right)^2 \right]^{0.5} \quad \text{(Eq. 1)}$$

3. Bedload transport

All the three components of seismic signals (two horizontal and one vertical) were collected. Each seismic station was composed of three geophones installed in a triangular array with two of them placed at about ca. 5 m from the river and the other one (the middle one) spaced out ca. 70 m towards the valley sidewalls, and following best practices described in Dietze et al. (2019). Data issued from geophones A were used to infer bedload flux, while data collected by the other geophones were used for cleaning the obtained timeseries (see below). Loggers were set at a sampling frequency of 400 Hz with an amplifier gain of 32.

The post-processing of collected seismic data to quantify bedload transport rates used the geophysical inversion model of Dietze et al. (2019) in the open source R package *eseis* (version 0.5.0) (Dietze, 2018). The principle consists of comparing the measured seismic spectra to a set of pre-calculated simulations of physical models predicting the spectra of fluvial turbulence and bed sediment transport. The FMI takes into account the two physical models to describe the seismic signals generated by water turbulence (Gimbert et al., 2014) and the motion of bedload particles on the riverbed (Tsai et al., 2012). These rely on a set of 15 constant site-specific parameters describing the sedimentological proprieties of bedload particles and of the fluid, the topography of the studied reach, the computational needs for the inversion and the seismic ground proprieties of the surveyed area (Table 2).

Table 2: Input parameters describing the FMI and calibrated values for both seismic stations.

	Parameter	**Symbol**	**GS1**	**GS2**
Sedimentological and fluid proprieties	D_{50} bedload grain diameter [m]	d_s	0.08	0.04
	Grain diameter standard deviation [log m]	s_s	1.1	1.4
	Sediment density [kg/m^3]	r_s	2650	2650
	Fluid density [kg/m^3]	r_w	1040	1040
Topography	Average channel width [m]	w_w	10	8
	Channel slope [rad]	a_w	0.03	0.02
	Distance river center to sensor [m]	r_0	10	11
Computational	Reference frequency [Hz]	f_0	1	1
	Model frequency range [Hz]	f	20-70	20-90
Seismic ground proprieties	Material quality factor at f_0 [-]	q_0	32.84	32.14
	Rayleigh wave phase velocity at f_0 [m/s]	v_0	197	4550.9
	Variation coefficient for v_0 [-]	p_0	0.43	0.95
	Q increase with frequency [-]	e_0	0.02	0.004
Variables	Bedload flux [kg/ms]	q_s	0.001 - 10	0.001 - 10
	Water depth [m]	h_w	0.3 - 1	0.3 - 1

These parameter values were quantified directly in the field, or extracted from previous studies, as was the case for both sediment (r_s) and fluid (r_w) densities which were retrieved from Dietze et al. (2019). The three parameters describing the topography of the seismically monitored stream reaches (w_w, a_w and r_0) were quantified using dGPS measurements, while the computational ones are set according to conventional seismic rules (f_0) and quality of the collected data (f). This latter parameter was determined looking at the shape of the empiric spectra recorded in periods having different hydraulic conditions in terms of water stage and bedload transport rates. The median diameter of moving bedload particles (d_s) and their

standard deviation (s_s) were quantified using a log-raised cosine distribution function following Tsai et al. (2012) to take into account the disproportionately large effect of larger grain sizes that have on the signal compared to smaller ones because of the higher vertical impact velocity when they are moving (hopping) in contact with the riverbed.

The seismic ground properties are used in the Green's function (Eq. S2; Aki and Richards, 2002; Burtin et al., 2016; Bakker et al., 2020) and they describe the way in which seismic waves propagate through the ground (v_0 and p_0), and the attenuation imposed by the medium on the carried seismic magnitude (q_0 and e_0).

$$u(f,x) = 2\pi f F(f,x_0) G(f,x,x_0) \quad \text{(Eq. 2)}$$

Where:

u(f,x) = seismic signal ground velocity at frequency f and at a distance x from the source
F(f, x_0) = Fourier transform of the magnitude at a given temporal period t
G(f,x,x_0) = Greens function converting force to ground velocity and describing the frequency-dependent wave attenuation related to proprieties of the medium through which the seismic waves have passed. Under the assumption that seismic forces impact orthogonal against the seismic device and that Rayleigh surface waves are the main excited waves, G can be expressed as (e.g. Sanchez-Sesma et al., 2011):

$$G(f,x,x_0) = \frac{k}{8 p_s v_p v_g} \sqrt{\frac{2}{\pi k r} e^{-\pi f r/(v_g Q)}} \quad \text{(Eq. 3)}$$

Where:

p_s = volumetric mass density of the medium [kg/m^3]
v_p = seismic wave phase velocity at f_0 [m/s]
v_g = seismic wave group velocity [m/s]
k = angular wavenumber ($k = 2\pi f/v_c$)
r = distance seismic source-receiver ($|x-x_0|$) [m]
Q = quality factor [-]

We determined seismic ground parameter values for the study area combining active tests (e.g. Bakker et al., 2020) with a Generalized Likelihood Uncertainty Estimation (GLUE) approach allowing to calibrate these unknown parameter values statistically.

Once the FMI was calibrated, the inversion process to convert seismic date into bedload flux and water stage was applied following Dietze (2018). First, the raw vertical component of the seismic records for the entire period of investigation collected by geophones A was de-convoluted, de-trended and finally clipped according to a pre-defined time step t_i (3 minutes in our case) in order to be converted into the frequency domain to produce a series of observed seismic spectra. Second, the two physical models describing the seismic activity related to flow turbulence (Gimbert et al., 2014) and bedload transport (Tsai et al., 2012) were used into a Monte Carlo simulation to produce a series of synthetic spectra describing different potential seismic conditions occurring in the monitored river reach that serve as a lookup table during the inversion process. This was achieved keeping all parameters values constant, but allowing for random variation of the two unknown parameters of interest (i.e. bedload flux and water depth) within pre-defined possible ranges (Table 2). As bedload transport is an unsteady variable over time, to enhance the representation of all possible seismic conditions that may have occurred, the FMI allows production of synthetic spectra with and without bedload transport. The inversion is then computed by comparing the observed and the synthetic spectra: for each spectrum measured at time t_i, the synthetic one having the lowest RMS error is kept and the associated instantaneous bedload flux and water depth values are retrieved from the lookup table. Inverted and measured water stage records were compared to evaluate both quality and reliability of model parametrization (Mancini et al., 2023).

Inferred bedload transport rates were cleaned from potential interferences with unwanted seismic sources such as anthropogenic noise (e.g. hikers and operator footsteps, as well as seismic noise generated by other scientific activities taking place in the forefield) or due to other geomorphic processes (e.g. mass movements) occurring on adjacent hillslopes. We investigated the source of every single transport peak to be sure that they were effectively related to riverine processes. We extracted the temporal occurrence of these events and we localized the seismic source by applying the *signal_migrate* function (also available in the *eseis* R-package; Dietze, 2018) thanks to our triangular array of geophones used at each monitoring station. This allowed us to sort the signal into two origins: if the estimated source was located into or close to the nearest channel we kept the inversion result, in the opposite case we discarded it. Then, we also discarded results matching with the occurrence of strong seismic activates exciting the entire range of considered frequencies in power spectral density plots as due to activities occurring in close proximity to geophones (e.g. wild animals) re-interpolating bedload flux timeseries using a moving mean operator (window size of 20 elements). Finally, bedload flux estimations in kg/ms are converted into kg/s multiplying them by the average channel width (10 m in GS1 and 8 m in GS2, Table 2), and interpolated at the same frequency of suspended sediment records (i.e. 2 minutes).

As the main parameters controlling FMI performance are those describing seismic ground proprieties, bedload flux uncertainty was assessed using Latin Hypercube Sampling (LHS; McKay, 1992) applied to q_0, v_0, p_0, e_0 and s_s parameters (Table 2). This method consists of randomly sampling within a hypercube having the same dimensions of the investigated variables (in this case 5), in our case four, in a way that every combination of parameter value can be sampled only once. Ground seismic parameter ranges are based on both mean and standard deviation of the best 100 simulations used to define final parameter values, while that for s_s is defined as the standard deviation obtained from the probabilistic log-raised cosine function. We generated a total of 1000 possible combinations and we classified ground seismic parameter sets according to a normal distribution in 5 different classes of standardized lengths for each parameter space. A total of 20 possible combinations (5 per parameter, one per each class associated to a specific s_s value) are selected and implemented into the FMI to produce several time series of bedload flux. Each set of inversion took about two weeks for a whole melt season on a high performance computer, and this justifies our choice to limit the total number of inversions. To assess whether or not this was sufficient, we looked at the ranges of predictions for these 20 inversions. In all cases the inversion with the optimized parameter set fell with the range of the 20 uncertainty inversions. However, these included some parameter sets with poor fit to the reference spectrogram. Thus, we used the RMSE fit to the reference spectrogram to identify the best 5 inversions and then we took for each time period the highest and lowest inverted bedload transport rate. These optimized transport rate fell within the range defined by the maxima and minima for GS1 in 2020 and 2021 and GS2 in 2020, and thus they were deemed as behavioral and providing a basic uncertainty estimation. For GS2 in 2021 the optimized transport rate was higher than the maximum and so for that time series we considered the best 6 inversions.

4. Data details

The datasets are composed by:

- Raw hourly 3-components collected seismic data in SAC format. Folder structure is composed by year, Julian day, hourly data in UTC. File names are denoted as station ID (OTM1 for GS1 and OTM2 for GS2), Julian day, hour, minute, second, channel and file name format.
- Text files of discharge, suspended sediment loads and bedload rates used in this study. Data are organized in the following way:
  Column 1 = Time in Julian day
  Column 2 = Suspended sediment flux in GS1 [kg/s]

Column 3 = Bedload flux in GS1 [kg/s]
Column 4 = Suspended sediment flux in GS2 [kg/s]
Column 5 = Bedload flux in GS2 [kg/s]

5. References

Aki, K. & Richards, P. G. (2002). *Quantitative Seismology*. University Science Book.

Bakker, M., Gimbert, F., Geay, T., Misset, C., Zanker, S. & Recking, A. (2020). Field Application and Validation of a Seismic Bedload Transport Model. *Journal of Geophysical Research: Earth Surface*, 125(5). https://doi.org/10.1029/2019JF005416

Beaton, A.E. & Tukey, J.W. (1974). The fitting of power series, meaning polynomials, illustrated on band-spectroscopic data. *Technometrics*, 16, 147-85. https://doi.org/10.2307/1267936

Burtin, A., Hovius, N. & Turowski, J. M. (2016). Seismic monitoring of torrential and fluvial processes. *Earth Surface Dynamics*, 285–307. https://doi.org/10.5194/esurf-4-285-2016

Dietze, M. (2018). The R package "eseis" – a software toolbox for environmental seismology. *Earth Surface Dynamics*, 6(3), 669–686. https://doi.org/10.5194/esurf-6-669-2018

Dietze, M., Gimbert, F., Turowski, J. M., Stark, K. A., Cadol, D. & Laronne, J. B. (2019). *The seismic view on sediment laden ephemeral flows—Modelling of ground motion data for fluid and bedload dynamics in the Arroyo de los Pinos* [Computer software manual]. Retrieved from http://micha-dietze.de/pages/publications/other/Dietze_et_al_2019b.pdf (Paper to SEDHYD conference)

Gimbert, F., Tsai, V. C. & Lamb, M. P. (2014). A physical model for seismic noise generation by turbulent flow in rivers. *Journal of Geophysical Research: Earth Surface*, 119(10), 2209–2238. https://doi.org/10.1002/2014JF003201

Mancini, D., Dietze, M., Müller, T., Jenkin, M., Miesen, F., Roncoroni, M., Nicholas, A. & Lane, S.N. (2023). Filtering of the signal of sediment export from a glacier by its proglacial forefield. *Geophysical Research Letters*.

McKay, M.D. (1992). Latin hypercube sampling as a tool in uncertainty analysis of computer models. *Proceedings of the 24th conference on winter simulation*, 557-564. https://doi.org/ 10.1145/167293.167637

Müller, T. & Miesen, F. (2022). *Stream discharge, stage, electrical conductivity & temperature dataset from Otemma glacier forefield, Switzerland (from July 2019 to October 2021)* [Data set]. Zenodo. https://doi.org/10.5281/zenodo.6202732

Sanchez-Sesma, F.J., Weaver. R.L., Kawase, H., Matsushima, S., Luzon, F. & Campillo, M. (2011). Energy partition among elastic waves for dynamic surface loads in a semi-infinite solid. *Bulletin of the Seismological Society of America*, 101, 1704-1709. https://doi.org/10.1785/0120100196

Taylor. J.R. (1997). *An Introduction to Error Analysis: The Study of Uncertainties in Physical Measurements*. University Science Books: Sausalito.

Tsai, V. C., Minchew, B., Lamb, M. P. & Ampuero, J.-P. (2012). A physical model for seismic noise generation from sediment transport in rivers. *Geophysical Research Letters*, 39(2). https://doi.org/10.1029/2011GL050255